Mechanics of Materials 42 (2010) 63–71

Contents lists available at ScienceDirect

Mechanics of Materials

journal homepage: www.elsevier.com/locate/mechmat

Stress–oxidation interaction in selective oxidation of Cr–Fe alloys

Honggang Zhou [a], Jianmin Qu [a,b,*], Mohammed Cherkaoui [a,b]

[a] School of Mechanical Engineering, Georgia Institute of Technology, 801 Fest Dr., Atlanta, GA 30322 – 0405, USA
[b] UMI 2958 GT-CNRS, Metz 57000, France

ARTICLE INFO

Article history:
Received 19 January 2009
Received in revised form 17 September 2009

Keywords:
Cr–Fe alloys
Oxidation
Stress
Couple

ABSTRACT

Metal oxidation is sustained by continuous diffusion of ions in the scale layer. At the same time, stresses are induced in the scale layer and the base metal due to internal oxidation and volumetric change when metal ions are oxidized. Such stress may in return affect the diffusion of ions in the oxide layer, thus changing the oxidation kinetics. In this paper, a continuum thermodynamic model is developed to account for such stress–diffusion interaction in the oxidation of Cr–Fe alloys. The model predicts that the compressive stress in the scale layer has a rather nonlinear distribution across the layer thickness with its maximum at the metal–scale interface. Such stress significantly slows down the rate of oxidation. Consequently, the growth kinetic is not strictly parabolic. It is found that the distribution of stress and diffusive ions in the scale layer can be normalized by the oxidation rate constant so that, with proper scaling, the numerical solutions given in this paper are applicable to any value of the rate constant.

1. Introduction

Growth of oxide scale on metallic alloys may cause significant mechanical stress in the scale layer. In return, such stress may affect the oxidation kinetics and may also lead to scale spallation or detachment (Noden et al., 1968; Rhines and Wolf, 1970; Stringer, 1970). Mechanisms of stress generation in the scale may include heteroepitaxy (Pieraggi and Rapp, 1988), Pilling and Bedworth Ratio (PBR) of conversion from metal into scale (Huntz, 1988; Kofstad, 1989), oxygen incorporation in substrate or reaction composition of oxygen and metal, nonstoichiometric vacancy concentration in the scale, etc. Among these, the PBR, the ratio of the oxide molar volume to that of the metal (Huntz, 1988; Kofstad, 1989), is believe to be primarily responsible for the generation of stresses during selective oxidation (Huntz, 1995), although oxygen incorporation in substrate or reaction composition of oxygen and metal may also introduces significant stresses in certain alloys.

Although mechanisms of oxidation-induced stresses have been studied extensively, very few attempts have been made to develop computational models to describe the oxidation–stress interaction process (Clarke, 2003; Krishnamurthy and Srolovitz, 2004; Limarga et al., 2004). Most of the existing models are based on the original concept of Rhines and Wolf (1970). Clarke (2003) considered the generation of lateral growth strain in response to the counter-diffusion of cations and anions. By neglecting stress relaxation, they have shown that the lateral growth strain rate is proportional to the outward cation flux. Under a steady-state condition, Limarga et al. (2004) derived the average growth stress by assuming that the inward oxygen diffusion occurs along grain boundaries. A more general model describing the stress distribution in the oxide scale is presented by Krishnamurthy and Srolovitz (2004), in which they had formulated a continuum framework that predicts the oxide scale growth rate and the spatial distribution of stress and concentrations within the scale. The stresses affect internal oxidation by changing the free energy of the reaction and affect diffusion by modifying the chemical potential. This allows the authors to consider how the stress inhibits internal oxidation in a thermodynamically and kinetically consistent manner.

* Corresponding author. Present address: Department of Civil and Environmental Engineering, Northwestern University. Tel.: +1 404 894 5687; fax: +1 404 894 0186.
E-mail address: jianmin.Qu@me.gatech.edu (J. Qu).

0167-6636/$ - see front matter © 2009 Elsevier Ltd. All rights reserved.
doi:10.1016/j.mechmat.2009.09.007

In this work, we follow closely the approach of Krishnamurthy and Srolovitz (2004) with a few notable differences. In our approach, the equations are formulated and solved in the Eulerian framework. One of the advantages of the Eulerian formulation is to allow the oxide lattice to "flow" upward, avoiding the complexity of computing the velocities of metal–scale and scale–air interfaces and greatly simplified the equations and their numerical solution. Another important difference is the use of a fully coupled theory (Swaminathan et al., 2007) between chemical reaction and mechanical stress, namely, not only oxidation induces stress, in return stress also affects the rate of oxidation. Furthermore, in this fully coupled theory, not only the hydrostatic stress, but also the deviatoric stress needs to be considered. Details of these differences and their consequences will be explained later in this paper.

To develop our model, a binary alloy (16% wt Cr–Fe) is used in this paper as a model material. It will be seen from the derivation that the general approach presented here is applicable to a wide range of alloys.

2. Model synopsis and assumptions used

Consider a Cr–Fe binary alloy exposed to an oxygen gas environment (e.g., air) with a given oxygen partial pressure at elevated temperature. Based on experimental data (Seo et al., 1986; Wood et al., 1966), it is reasonable to assume that at over 800 °C the only oxidation product forming a scale layer on the alloy surface is Cr_2O_3. Observations from experiments (Hultquist et al., 1986; Seo et al., 1986; Wood et al., 1966) give two different scale morphologies for oxidation of Cr–Fe alloys at different temperature regions. Below 500 °C, a layer of Fe_2O_3 exists on the top of the oxide film (Hultquist et al., 1986). Above 800 °C, though some Fe_2O_3 is observed at the very early stage of oxidation, Cr_2O_3 is by far the dominant compound in the oxide film at steady state (Seo et al., 1986; Wood et al., 1966).

The very initial stage of oxidation process, which includes numerous different physical and chemical processes, is extremely complicated. To date, there is no consistent agreement on the formation mechanism of the very first layer of oxide. To avoid such complexity, this paper models the oxidation process only after an infinitesimally thin scale layer had already formed. For simplicity, we assume that the initial scale layer is Cr_2O_3 with a perfect (defect free) lattice structure.

When such a metal–oxide system is further exposed to a given oxygen partial pressure at elevated temperature, a layer of atomic oxygen will be adsorbed to the scale surface (Atkinson, 1985). According to Cabrera and Mott (Cabrera and Mott, 1948), the adsorbed oxygen layer is atomic. These oxygen atoms are then ionized by capturing the free electrons in the scale layer. At the same time, oxidation-favored Cr atoms in the binary alloy are converted to ions at the metal/scale interface. Consequently, counter diffusion occurs, namely, both oxygen anion O'' at the gas–scale interface and the chromium cation $Cr^{\cdot\cdot\cdot}$ at the metal–scale interface will diffuse into the scale layer driven by electrochemical potentials across the scale layer. When two $Cr^{\cdot\cdot\cdot}$ meet with three O'', oxidation reaction may take place to form a Cr_2O_3. Depending on the rates of diffusion of these reactive ions, new oxide may form near the metal–scale interface, the gas–scale interface or within the scale layer. Once formed, the Cr_2O_3 lattice is assumed non-diffusible, although they can be transported due to the subsequently created new Cr_2O_3 sites.

As discussed in the previous section, the diffusion paths and the mechanism of internal oxidation in polycrystalline oxides may be rather complex, and the locations of new oxide within the existing scale layer may vary depends on the material system. Nevertheless, effective diffusivities of diffusing ions can be used to account for both grain boundary and lattice diffusion by assuming that the scale layer is a homogeneous continuum. Clearly, such a continuum assumption also conveniently homogenizes the internal oxidation, namely, new Cr_2O_3 sites can be created anywhere within the oxide layer.

In the Cr_2O_3 scale, $Cr^{\cdot\cdot\cdot}$ cations diffuse much faster than Fe ions (Hoshino and Peterson, 1985; Lobnig et al., 1992). Therefore, it is assumed that the diffusion of Fe in the scale layer is negligible. Furthermore, we assume that O ions do not diffuse into the metal. Therefore, in our model, the metal–scale interface is physically identified as the boundary between regions without Fe and without O, respectively.

At the metal–scale interface, Cr atoms in the metal alloy are striped of their electrons, and the resulting $Cr^{\cdot\cdot\cdot}$ cations jump across the metal–scale interface into the scale layer driven by the electrochemical potential. This leaves behind Cr vacancies in the metal alloy near the metal–scale interface. The higher Cr vacancy concentration near the metal–scale interface compels Cr atomic diffusion in the metal alloy toward the interface. Although the metal substrate is assumed to be infinitely thick so that the supply of Cr is infinite, experiments (Hultquist et al., 1986; Seo et al., 1986) indicate that local (near interface on the metal side) Cr depletion occurs. This means that the rate of converting Cr atoms into $Cr^{\cdot\cdot\cdot}$ cations is faster than that of Cr atomic diffusion in the metal alloy.

The decreasing Cr (or increasing Cr vacancy) concentration in the metal near the scale–metal interface typically generates tensile stress in the metal. In addition, internal oxidation increases the volume of the oxide scale not only in the thickness direction, but also in the plane of the scale layer. The latter induces additional stress in the scale and the metal substrate.

A key element of the current model is the stress-dependent chemical potentials for the various species involved. Such stress-dependent chemical potentials affect the oxidation process in two ways. First, they introduce the stress into the diffusion equations so the fluxes are stress-dependent as well. Second, they bring the stress into the total free energy of the system, which controls the rate of oxidation/reduction reaction. Without the influence of stress, the rate of chemical reaction is dictated solely by the concentrations of reactants and products. When mechanical stress is involved, the elastic strain energy becomes a part of the total free energy. A chemical reaction can take place only if the total free energy is to be reduced. In other word, even if a chemical reaction reduces the total chemical

energy, it may not take place unless the amount of reduction in chemical energy is more than the increase in mechanical (strain) energy.

Having described the basic framework of the model, we proceed to derive the appropriate governing equations and boundary/initial conditions.

3. Governing equations

Shown in Fig. 1 is a schematic of the metal–scale–oxygen structure, where a Cartesian spatial (Eulerian) coordinate system x_i ($i = 1, 2, 3$) has been introduced so that the metal–scale interface is located at $x_3 = 0$. During the entire oxidation process, this coordinate system is treated as a reference frame fixed to the metal–oxide interface. All the governing equations and boundary conditions will be presented in this Eulerian coordinate system.

When writing the field quantities related to deformation such as strain and stress, it is often convenient to introduce the Lagrangian reference frame X_i ($i = 1, 2, 3$). We assume in this paper that X_i coincide with x_i initially at $t = 0$. The two coordinates are related by

$$\mathbf{x} = \mathbf{X} + \mathbf{U}(\mathbf{X}, t) \quad \text{or} \quad \mathbf{X} = \mathbf{x} - \mathbf{U}(\mathbf{X}(\mathbf{x}), t) = \mathbf{x} - u(\mathbf{x}, t), \tag{1}$$

where $\mathbf{U}(\mathbf{X}, t)$ is the particle displacement of the particle $\mathbf{X}$, while $u(\mathbf{x}, t)$ can be interpreted as the displacement of the particle instantaneously located at $\mathbf{x}$.

3.1. Kinematic equations

The total deformation gradient tensor $\mathbf{F}$ is related to the displacement vector $\mathbf{U}(\mathbf{X}, t)$ through

$$\mathbf{F} = \mathbf{F}^e\mathbf{F}^c = \mathbf{I} + \nabla_X\mathbf{U}, \quad \text{or} \quad \mathbf{F}^{-1} = (\mathbf{F}^e\mathbf{F}^c)^{-1} = \mathbf{I} - \nabla\mathbf{u}. \tag{2}$$

The eigentransformation due to compositional change is given by

$$\mathbf{F}^c = J^{c1/3}\mathbf{I} = \sqrt{1 + 2\sum\nolimits_s \eta_s \Delta c_s}\,\mathbf{I}. \tag{3}$$

where η_s is the coefficients of compositional expansion (CCE) and Δc_s is the deviation of molar fraction of c_s from its stoichiometric composition (Swaminathan et al., 2007).

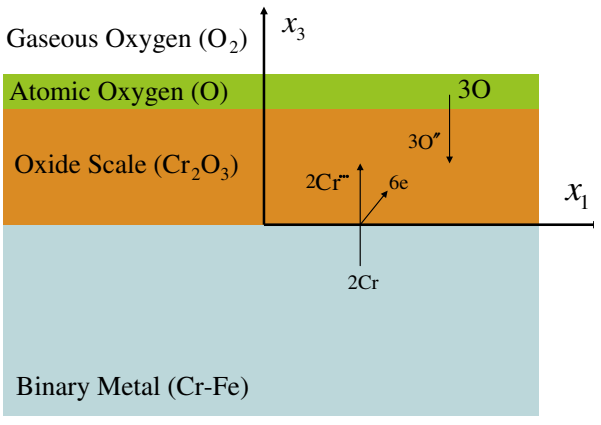

Fig. 1. Schematic of the metal–oxide–gas structure (not to scale).

For the oxidation problem considered here, there are several species in the scale layer $0 \leqslant x_3 \leqslant h$ that may change their compositions. They are, respectively, $Cr^{\cdots}$ ($s = Cr$), O'' ($s = O$) and Cr_2O_3 ($s = p$), due to the formation of oxide from $Cr^{\cdots}$ and O''. For Cr_2O_3, we have $\eta_p = (2 + 3)/3 = 5/3$, while $\eta_{Cr^{\cdots}}$ and η_O can be measured experimentally or computed using molecular dynamic simulations (Swaminathan and Qu, 2009). In the metal ($x_3 < 0$), chromium atom ($s = Cr(a)$) is the only independent diffusible species.

It then follows from the second of (2) that

$$\mathbf{F}^e = (\mathbf{I} - \nabla\mathbf{u})^{-1} \cdot \mathbf{F}^{c^{-1}} = \frac{\mathbf{I} - \nabla\mathbf{u}^{-1}}{\sqrt{1 + 2\sum_s \eta_s \Delta c_s}}, \tag{4}$$

$$\begin{aligned}\mathbf{E}^e &= \frac{1}{2}[(\mathbf{F}^{e^T}\mathbf{F}^e - \mathbf{I}] \\ &= \frac{1}{2}\left[\frac{1}{1 + 2\sum_s \eta_s \Delta c_s}[(\mathbf{I} - \nabla\mathbf{u})^{-1}]^T(\mathbf{I} - \nabla\mathbf{u})^{-1} - \mathbf{I}\right].\end{aligned} \tag{5}$$

3.2. Kinetic equations

The mechanical stresses in both the oxide scale and the metal substrate must satisfy the equilibrium equations. In terms of the first Piola–Kirchhoff stress tensor, the equilibrium equations can be written as

$$\nabla_X \cdot \boldsymbol{\sigma}^0 = (\nabla_x \cdot \boldsymbol{\sigma}^0) : \mathbf{F} = 0, \tag{6}$$

where the first gradient operator is with respect to the Lagrangian coordinates $\mathbf{X}$ and the second one is with respect to the spatial coordinates $\mathbf{x}$ as indicated by the subscript. Making use of the Hooke's law, one can express the first Piola–Kirchhoff stress tensor in term of the deformation gradients,

$$\boldsymbol{\sigma}^0 = \mathbf{C} : \mathbf{E}^e \cdot \mathbf{F}^T, \tag{7}$$

where $\mathbf{C}$ is the elastic stiffness tensor. In this paper, it is assumed that $\mathbf{C}$ is independent of Δc_s.

3.3. Stress-dependent chemical potential

Strictly speaking, electrochemical potentials should be used for the oxidation process. However, if local electroneutrality is assumed (as done in this paper), the diffusion process can be described using the chemical potential alone (Swaminathan et al., 2007). For most insulating and semi-conducting ceramics, local electroneutrality is an excellent assumption throughout the film, except for thin surface layers of a few nanometers (Dechamps and Barbier, 1991; Krishnamurthy and Srolovitz, 2003). The stress-dependent chemical potential for a species s in ionic solids has been derived in by Swaminathan et al. (2007),

$$\mu_s = \mu_s^0 + RT \ln c_s + V_s^m \tau_s \tag{8}$$

where μ_s^0 is the chemical potential of species s at some reference state, R and T are the universal gas constant and temperature, respectively, V_s^m is the molar volume of species s in its nature (stress-free stoichiometric state). The last term in (8) is the stress-dependent part of the chemical potential derived in (Swaminathan et al., 2007). If one

assumes that the elastic stiffness tensor is independent of concentration, then τ_s reduces to

$$\tau_s = \eta_s\left(\frac{3}{2}\mathbf{E}^e : \mathbf{C} : \mathbf{E}^e - \frac{1}{J^c}\mathrm{tr}[\mathbf{F}\cdot\boldsymbol{\sigma}^0]\right), \tag{9}$$

where $J^c = ||\mathbf{F}^c||$ is the Jacobian of the deformation gradient tensor, and $\mathbf{E}^e$ is the elastic strain given by (5).

3.4. Oxidation–reduction reaction in the scale layer ($0 \leqslant x_3 \leqslant h$)

During oxidation, every two $Cr^{\cdot\cdot\cdot}$ and three O'' will form a chromium oxide (chromina) Cr_2O_3, or vice versa, i.e.,

$$2Cr^{\cdot\cdot\cdot} + 3O'' \leftrightharpoons Cr_2O_3. \tag{10}$$

Statistically speaking, both oxidation (forward) and reduction (backward) reactions may take place simultaneously. When the forward reaction is more favorable, there is a net increase of the product (Cr_2O_3). The newly formed oxide creates new lattice sites leading to scale growth. This is possible if and only if the forward reaction decreases the total free energy, i.e.,

$$dG = d\mu_p - 2d\mu_{Cr} - 3d\mu_O < 0, \tag{11}$$

where μ_{Cr}, μ_O and μ_p are, respectively, the chemical potentials of $Cr^{\cdot\cdot\cdot}$, O'' and the product Cr_2O_3. Clearly, chemical equilibrium is achieved when $dG = 0$.

It follows from the chemical Eq. (10) that the rate of forward reaction is given by $k_f c_{Cr}^2 c_O^3$, and the rate of backward reaction is given by $k_b c_p$, where k_f and k_b are the reaction rate constants of the forward and backward reactions, respectively. Therefore, the net rate of increase of the product is given by

$$R_p = k_f c_{Cr}^2 c_O^3 - k_b c_p. \tag{12}$$

At chemical equilibrium, the net rate should be zero.

Since the chemical potentials are stress-dependent, it can be easily shown that the reaction rate constants k_f and k_b are stress-dependent,

$$k_f = k_f^0 \exp\left[-\frac{V_p^m \tau_p}{RT}\right], \quad k_b = k_b^0 \exp\left[-\frac{2V_{Cr}^m\tau_{Cr} + 3V_O^m\tau_O}{RT}\right], \tag{13}$$

where k_f^0 and k_b^0 are, respectively, the forward and backward reaction rate constants when there is no mechanical stress.

3.5. Diffusion and fluxes

In the scale layer ($0 \leqslant x_3 \leqslant h$), it is assumed that the oxide (product) does not diffuse, although its lattice may still move (convection) due to internal oxidation. The diffusion fluxes of $Cr^{\cdot\cdot\cdot}$ and O'' are related to their chemical potentials through

$$\mathbf{J}_s = -\frac{D_s c_s}{RT}\nabla\mu_s, \quad \text{for } s = \mathrm{Cr} \text{ and } \mathrm{O} \tag{14}$$

where ∇ is the gradient operator with respect to the spatial coordinates $\mathbf{x}$, and D_s is the effective diffusivity of specie s in the oxide scale. Substitution of (8) into (14) yields,

$$\mathbf{J}_s = -\frac{D_s c_s}{RT}\left[RT\frac{\nabla c_s}{c_s} + V_s^m \nabla\tau_s\right], \quad \text{for } s = \mathrm{Cr} \text{ and } \mathrm{O} \tag{15}$$

Similarly, in the metal substrate ($x_3 < 0$), diffusion flux of chromium is given by

$$\mathbf{J}_{Cr(a)} = -\frac{D_{Cr(a)} c_{Cr(a)}}{RT}\left[RT\frac{\nabla c_{Cr(a)}}{c_{Cr(a)}} + V_{Cr(a)}^m \nabla\tau_{Cr(a)}\right], \tag{16}$$

where $D_{Cr(a)}$ is the diffusivity of atoms in the metal alloy.

It is noted that the mass diffusion and their fluxes discussed above are the mass motion relative to a background lattice. In the scale layer, this background lattice is the Cr_2O_3 lattice already formed. In the metal substrate, this background lattice is the original Cr–Fe lattice.

3.6. Continuity equation

When new oxide is created near the scale–metal interface, or internally within the scale layer, the existing Cr_2O_3 lattice will move up to accommodate the new lattice sites. Therefore, the motion of a diffusible species in the oxide scale consists of both diffusion relative to the background lattice and the transport of the background lattice itself. This situation is called convective diffusion (Levich, 1962). The continuity equation in a fixed coordinate (Eulerian description) system for the product is thus given by

$$\frac{\partial c_p}{\partial t} = R_p - \nabla\cdot(c_p\mathbf{v}). \tag{17}$$

where R_p is the net rate of oxide generation given by (12), and $\mathbf{v} = \mathbf{v}(\mathbf{x}, t) = \partial\,\mathbf{u}(\mathbf{x}, t)/\partial t$ is the spatial velocity distribution given as a function of time t and the Eulerian coordinates $\mathbf{x}$. The left hand side of (17) is the change of product concentration. It equals the rate of product generation plus the net flow (convection) due to the transport of the existing background lattice. This convective term is necessary because convection may also change the concentration locally at a fixed spatial location. The inclusion of this convective term in (17) is one of the major differences between the present model and that of (Krishnamurthy and Srolovitz, 2004).

For the diffusing ions, the mass transport due to diffusion needs to be included in the continuity equation. Thus, the continuity equations for $Cr^{\cdot\cdot\cdot}$ and O'' become

$$\frac{\partial c_{Cr}}{\partial t} = -2R_p - \nabla\cdot J_{Cr} - \nabla\cdot(c_{Cr}\mathbf{v}), \tag{18}$$

and

$$\frac{\partial c_O}{\partial t} = -3R_p - \nabla\cdot J_O - \nabla\cdot(c_O\mathbf{v}). \tag{19}$$

In other words, the time–rate of change of the ion concentration equals to the local consumption ($-2R_p$ for $Cr^{\cdot\cdot\cdot}$ and $-3R_p$ for O''), plus the diffusion and the convection.

In the metal substrate, the only contribution to the local rate of change of Cr concentration comes from diffusion. Thus, the continuity equation becomes

$$\frac{\partial c_{Cra}}{\partial t} = -\nabla\cdot\mathbf{J}_{Cr_{(a)}} \tag{20}$$

3.7. Boundary value problem

Consider the oxide scale first. It follows from (2)–(5) that $\boldsymbol{\sigma}^0$, $\mathbf{F}^e$, $\mathbf{F}^c$ and $\mathbf{E}^e$ can be expressed in terms of the six unknown scalar functions $\mathbf{u}(\mathbf{x}, t)$ and $c_s(\mathbf{x}, t)$ for s = Cr, O and p. Making use of these relationships in the continuity conditions (17)–(19) and the kinetic condition (6) yields six partial differential equations for the six unknown scalar functions $\mathbf{u}(\mathbf{x}, t)$ and $c_s(\mathbf{x}, t)$ (s = Cr, O and p).

Similarly, in the metal substrate, it follows from (16), (20), (7), and (5) that $\boldsymbol{\sigma}^0$, $\mathbf{F}^e$, $\mathbf{F}^c$ and $\mathbf{E}^e$ can be expressed in terms of four unknown scalar functions $\mathbf{u}(\mathbf{x}, t)$ and $c_{\mathrm{Cr}(a)}(\mathbf{x}, t)$. Making use of these relationships in the continuity condition (20) and the kinetic condition (6) yields four partial differential equations for the four unknown scalar functions $\mathbf{u}(\mathbf{x}, t)$ and $c_{\mathrm{Cr}(a)}(\mathbf{x}, t)$.

With proper continuity conditions at the scale–air and metal–scale interfaces, and proper boundary conditions on the sides of the structure depicted in Fig. 1, these partial differential equations formulate a boundary value problem that can be solved to obtain the deformation, stresses and the defect concentration throughout the scale layer and the metal substrate, as well as the oxidation kinetics.

4. One-dimensional examples

To illustrate the utility of the model formulated above and to reveal certain fundamental features of the model predictions, we present some numerical examples in this section. To this end, we assume that all the material properties are independent of the ion concentration. Also, the scale layer and the metal substrate are assumed to be linearly elastic and isotropic solids with E_n and ν_n being the elastic constants for the oxide (n = 1) and the metal (n = 2). Furthermore, it is assumed that the elastic constants are independent of the defect concentration. This is valid for dilute ion concentrations.

Next, we assume that the boundary conditions on the vertical sides are such that the total width of the sample as shown in Fig. 1 remains the same, and the scale grows in the vertical (x_3) direction only. Consequently, $u_1 = u_2 = 0$, $u_3 = u_3(x_3, t)$ and c_s=$c_s(x_3, t)$. Therefore, the problem becomes effectively one-dimensional, and all the filed quantities depend on the vertical coordinate x_3 only.

To facilitate the numerical solutions, we introduce a length scale $\lambda = \sqrt{D_{\mathrm{Cr}}/k_f^0}$ and a time scale $\tau = 1/k_f^0$. The non-dimensional time, spatial coordinate and displacement can then be defined as,

$$\hat{x}_3 = \frac{x_3}{\lambda}, \quad \hat{u} = \frac{u}{\lambda}, \quad \hat{t} = \frac{t}{\tau}. \tag{21}$$

One advantage of such normalization is that the governing equations and boundary conditions become independent of k_f^0 when written in terms the above non-dimensional variables.

4.1. Governing equations in one-dimensional

For the specific one-dimensional problem considered in this section, it is easy to see that in both the scale layer and the metal substrate, the only non-zero stress components are $\sigma_{11}^0 = \sigma_{22}^0$. This leads to

$$\frac{\partial \hat{u}_3}{\partial \hat{x}_3} = \frac{1+\nu_1}{1-\nu_1}\sum_k \eta_k \Delta c_k \tag{22}$$

Consequently, in the scale layer, the continuity Eqs. (17)–(19) become

$$\frac{\partial c_{\mathrm{Cr}}}{\partial \hat{t}} = -2c_{\mathrm{Cr}}^2 c_{\mathrm{O}}^3 \exp\left(-\hat{\eta}_p \sum_s \eta_s \Delta c_s\right) + \frac{\partial^2 c_{\mathrm{Cr}}}{\partial \hat{x}_3^2} + \hat{\eta}_{\mathrm{Cr}} \frac{\partial}{\partial \hat{x}_3}\left[c_{\mathrm{Cr}} \sum_s \eta_s \frac{\partial c_s}{\partial \hat{x}_3}\right] - \frac{\partial}{\partial \hat{x}_3}\left(c_{\mathrm{Cr}} \frac{\partial \hat{u}_3}{\partial \hat{t}}\right), \tag{23}$$

$$\frac{\partial c_{\mathrm{O}}}{\partial \hat{t}} = -3c_{\mathrm{Cr}}^2 c_{\mathrm{O}}^3 \exp\left(-\hat{\eta}_p \sum_s \eta_s \Delta c_s\right) + \frac{D_{\mathrm{O}}}{D_{\mathrm{Cr}}} \frac{\partial^2 c_{\mathrm{O}}}{\partial \hat{x}_3^2} + \hat{\eta}_{\mathrm{O}} \frac{D_{\mathrm{O}}}{D_{\mathrm{Cr}}} \frac{\partial}{\partial \hat{x}_3}\left[c_{\mathrm{O}} \sum_s \eta_s \frac{\partial c_s}{\partial \hat{x}_3}\right] - \frac{\partial}{\partial \hat{x}_3}\left(c_{\mathrm{O}} \frac{\partial \hat{u}_3}{\partial \hat{t}}\right), \tag{24}$$

$$\frac{\partial c_p}{\partial \hat{t}} = c_{\mathrm{Cr}}^2 c_{\mathrm{O}}^3 \exp\left(-\hat{\eta}_p \sum_s \eta_s \Delta c_s\right) - \frac{\partial}{\partial \hat{x}_3}\left(c_p \frac{\partial \hat{u}_3}{\partial \hat{t}}\right), \tag{25}$$

where

$$\hat{\eta}_s = \frac{2V_s^m E_1 \eta_s}{RT(1-\nu_1)} \tag{26}$$

measures the coupling between stress and diffusion.

Furthermore, it follows from (7) and (9) that the non-zero stress components in the scale layer are

$$\sigma_{11}^0 = \sigma_{22}^0 = -\frac{E_1}{1-\nu_1}\sum_s \eta_s \Delta c_s, \tag{27}$$

and the stress-dependent part of the chemical potential is

$$\tau_s = \frac{2E_1\eta_s}{1-\nu_1}\sum_k \eta_k \Delta c_k. \tag{28}$$

In the metal substrate, the continuity Eq. (20) becomes

$$\frac{\partial c_{\mathrm{Cr}(a)}}{\partial \hat{t}} = \frac{D_{\mathrm{Cr}(a)}}{D_{\mathrm{Cr}}} \frac{\partial^2 c_{\mathrm{Cr}(a)}}{\partial \hat{x}_3^2} + \hat{\eta}_{\mathrm{Cr}(a)} \frac{D_{\mathrm{Cr}(a)}}{D_{\mathrm{Cr}}} \frac{\partial}{\partial \hat{x}_3}\left[c_{\mathrm{Cr}(a)} \eta_{\mathrm{Cr}(a)} \frac{\partial c_{\mathrm{Cr}(a)}}{\partial \hat{x}_3}\right]. \tag{29}$$

The non-zero stress components in the metal substrate are

$$\sigma_{11}^0 = \sigma_{22}^0 = -\frac{E_2}{1-\nu_2}\eta_{\mathrm{Cr}(a)} \Delta c_{\mathrm{Cr}(a)}. \tag{30}$$

And the corresponding stress-dependent part of the chemical potential is

$$\tau_{\mathrm{Cr}(a)} = \frac{2E_2\eta_{\mathrm{Cr}_{(a)}}}{1-\nu_2}\eta_{\mathrm{Cr}a} \Delta c_{\mathrm{Cr}a}. \tag{31}$$

It can be easily seen that the above stress fields automatically satisfy the equilibrium Eq. (6).

4.2. Boundary conditions

In addition to the governing equations above, interface conditions need to be specified. In the structure shown in Fig. 1, there are two interfaces, the metal–scale interface

and the scale–air interface. At these interfaces, the following conditions must be satisfied: (a) continuity of mass flux of each species, (b) continuity of chemical potential of each species for adsorption and ionization reaction, respectively, (c) continuity of displacement and (e) continuity of traction. These conditions are described below.

4.2.1. Metal–scale interface ($x_3 = 0$)

At the metal–scale interface, ionization of Cr atoms is assumed to be an equilibrium process. Thus, continuity of chemical potentials must hold between $Cr^{\cdot\cdot}$ ions and Cr atoms, i.e.,

$$\frac{\mu^0_{Cra} - \mu^0_{Cr}}{RT} + \ln\frac{c_{Cr_{(a)}}}{c_{Cr}} = \hat{\eta}_{Cr}\sum_k \eta_k \Delta c_k - \hat{\eta}_{Cra}\eta_{Cr(a)}\Delta c_{Cr(a)}. \quad (32)$$

Conservation of mass for Cr across the interface leads to

$$\frac{\partial c_{Cra}}{\partial \hat{x}_3} + \hat{\eta}_{Cr(a)}\left[c_{Cra}\eta_{Cr(a)}\frac{\partial c_{Cr(a)}}{\partial \hat{x}_3}\right] = \frac{D_{Cr}}{D_{Cr_{(a)}}}\frac{\partial c_{Cr}}{\partial \hat{x}_3} + \hat{\eta}_{Cr}\frac{D_{Cr}}{D_{Cr_{(a)}}}\left[c_{Cr}\sum_s \eta_s \frac{\partial c_s}{\partial \hat{x}_3}\right]. \quad (33)$$

Furthermore, per the assumption that noO″ can cross the interface into the metal, theO″ flux must cease at the interface, i.e.,

$$\frac{\partial c_O}{\partial \hat{x}_3} + \hat{\eta}_O\left[c_O\sum_s \eta_s \frac{\partial c_s}{\partial \hat{x}_3}\right] = 0. \quad (34)$$

Finally, traction continuity is automatically satisfied by the choice of stress components, and the continuity of displacement leads to

$$\hat{u}_3|_{\hat{x}_3=0^+} = \hat{u}_3|_{\hat{x}_3=0^-}. \quad (35)$$

4.2.2. At the scale–air interface ($\hat{x}_3 = h/\lambda$)

At the scale–air interface, equilibrium condition is assumed for ionization of oxygen (in the air), i.e.,

$$\frac{1}{2RT}\mu^0_{O_2} + \ln P^{1/2}_{O_2} = \frac{\mu^0_O}{RT} + \ln c_O + \hat{\eta}_O\sum_k \eta_k \Delta c_k. \quad (36)$$

Where $\mu^0_{O_2}$ is the standard chemical potential of oxygen gas and P_{O_2} is the oxygen partial pressure in the air. Note that h is not known a priori. It is a function of time that needs to be solved. In addition, since the $Cr^{\cdot\cdot}$ ion cannot leave the scale, its flux must follow the Stefan (Garcia and Kovacs, 1994) condition at the scale–air interface, i.e.,

$$\frac{\partial c_{Cr}}{\partial \hat{x}_3} + \hat{\eta}_{Cr}\left[c_{Cr}\sum_s \eta_s \frac{\partial c_s}{\partial \hat{x}_3}\right] = -c_{Cr}\frac{d\hat{u}_3}{d\hat{t}}. \quad (37)$$

Furthermore, it is assumed that, in comparison with the stresses in the scale layer, the atmosphere pressure is negligible in typical applications. Thus, the scale–air interface can be viewed as a traction free surface which is satisfied by the choice of the stress components.

An additional condition needed is $c_{Cr(a)} = C$ as $x_3 \to -\infty$. This is equivalent to assuming the Cr concentration is a constant deep inside the base metal.

5. Numerical solution procedure

In this paper, the governing equations above are solved by a finite-difference method. A very thin initial scale thickness $h(t)|_{t=0} = h_0 = 20$ nm is assumed initially. The material properties of 16% (wt) Cr–Fe alloy and its oxide used in the numerical simulation are listed in Table 1 (Hammer, 2002; Horiguchi and Shindo, 2003; Tsai et al., 1996; Yoshimura et al., 2004). Oxygen partial pressure is set to be 0.3 atm at the air–oxide interface. Furthermore, it is assumed that once the oxide is formed, it is stable and no reduction takes place. This means that backward reaction rate constant $k^0_b = 0$.

By substituting (22) into (23), (24), (25), and (29) to eliminate u_3, we arrive at four partial differential equations with four unknown functions. They are c_{Cr}, c_O, c_p in the oxide scale and $c_{Cr(a)}$ in the metal. These four equations were solved by an explicit finite-difference method. The time step used is $\Delta t = 1$ s . The initial scale layer of thickness h_0 was first divided evenly into $n = 3$ elements with $n + 1 = 4$ nodes across the thickness. At $t = 0$, all the quantities c_{Cr}, c_O, c_p are known throughout the initial scale layer, and $c_{Cr(a)}$ is known throughout the metal. Eqs. (23), (24), (25), and (29) can then be integrated with respect to time to obtain the values of c_{Cr}, c_O, c_p and $c_{Cr(a)}$ at the next time step, $t = \Delta t$. The integration constants are determined by the initial and boundary conditions. Once the values of c_{Cr}, c_O, c_p are known for $t = \Delta t$, the displacement $u_3(x, t)$ can be obtained from (22). Consequently, the scale thickness at $t = \Delta t$ is given by $h_1 = h_0 + u_3(h_0, \Delta t)$. The above process is then repeated N times to obtain the solutions at any desired time, $t = N\Delta t$.

6. Results and discussion

The scale thickness is plotted as the solid line in Fig. 2. The triangle symbols in Fig. 2 are the experimental results by Kurokawa et al. (2004). For comparison purpose,

Table 1
Material properties of 16% (wt) Cr–Fe alloy and its oxide.

	Symbol	Value
Chromia properties		
Chemical expansion coefficient	η_{Cr}	0.05
	η_O	0.02
	η_p	5/3
Diffusivity of chromium ion	D_{Cr}	5.8×10^{-16} cm^2/s
Diffusivity of oxygen ion	D_O	3.0×10^{-16} cm^2/s
Temperature	T	1073 K
Young's modulus	E	250 GPa
Poisson's coefficient	V	0.27
Molar volume	$V_p = M(Cr_2O_3)/\rho$	2.92×10^{-5} m^3/mol
16% (wt) Cr–Fe alloy properties		
Chemical expansion coefficient	$\eta_{Cr(a)}$	0.05
Diffusivity of vacancy	$D_{Cr(a)}$	6×10^{-16} cm^2/s
Young's modulus	E	162.3 GPa
Poisson's coefficient	V	0.29

numerical results without accounting for the stress–diffusion interaction are also plotted in the same figure as the dotted line. It is seen that neglecting the stress–diffusion interaction overestimates the scale thickness, particularly over longer time period. This is because the compressive stress developed in the scale layer can significantly reduce the diffusion of ions, thus slowing down the scale growth.

Shown in Fig. 3a is the stress distribution across the thickness of the scale layer at four different oxidation times. The thickness is measured from the metal–scale interface. The right end of the curves indicates the thickness of the scale when the stress distribution is measured. It is seen that spatially the maximum (compressive) stress occurs at the metal–scale interface, and decreases gradually away from it. Very near the air–scale interface, the stress decreases abruptly. The temporal evolution of the stress at several different locations within the scale layer is shown in Fig. 3b. It is seen that the compressive stress increases with time, and eventually saturates. For the example considered here, the maximum saturated compressive stress is about 2.6 GPa, occurring on the scale side of the metal–scale interface. Interestingly, the newly formed oxide starts with zero stress, increases very quickly within a few minutes to a somewhat saturated value. This is because when new oxide just formed, it is not fully dense yet. There is still room for adding more oxide before compressive stresses are fully developed. Once the density reaches a threshold value, stress will remain relatively constant. This result contradicts that of (Krishnamurthy and Srolovitz, 2003) where the numerical results seem to indicate that the stress at any point in the scale layer keeps increasing without bound.

To further illustrate the oxidation kinetics, the stress-dependent oxidation rate constant k_f as given by the first of (13) is plotted in Fig. 4 at four different locations in the scale. As expected, at a given location, the oxidation

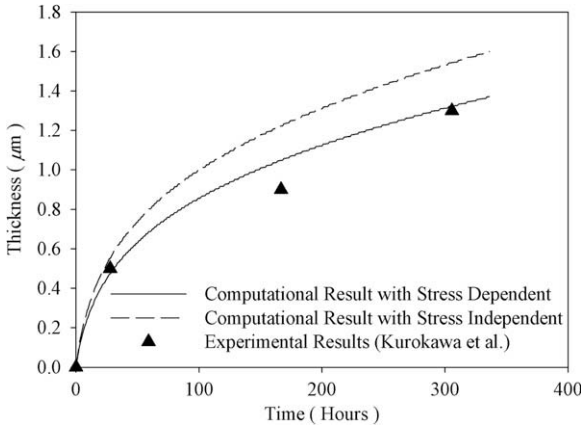

Fig. 2. Oxidation kinetics profile of 16% (wt) Cr alloy.

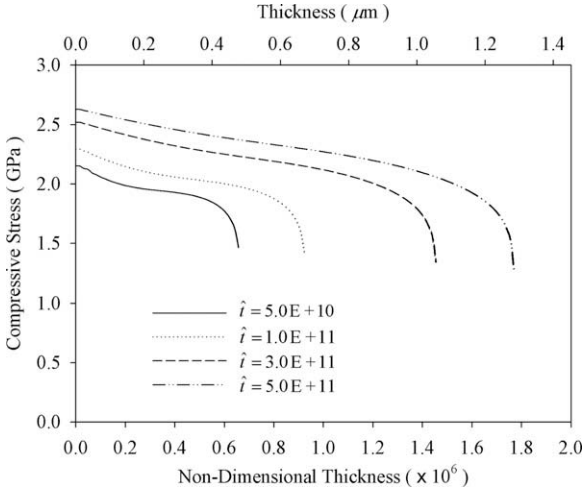

Fig. 3a. Stress distribution along scale thickness at different times.

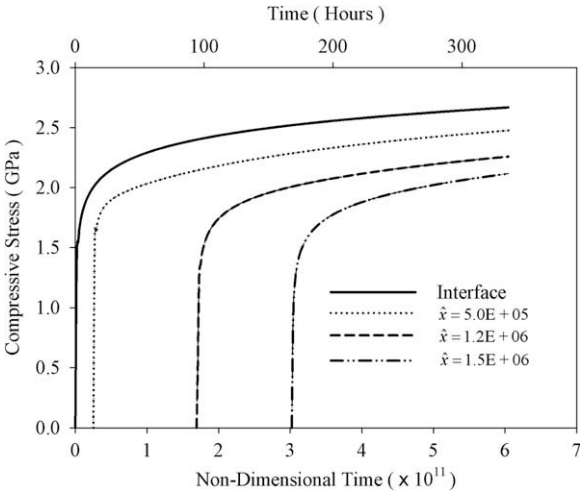

Fig. 3b. Stress evolution over time at different locations within the scale layer.

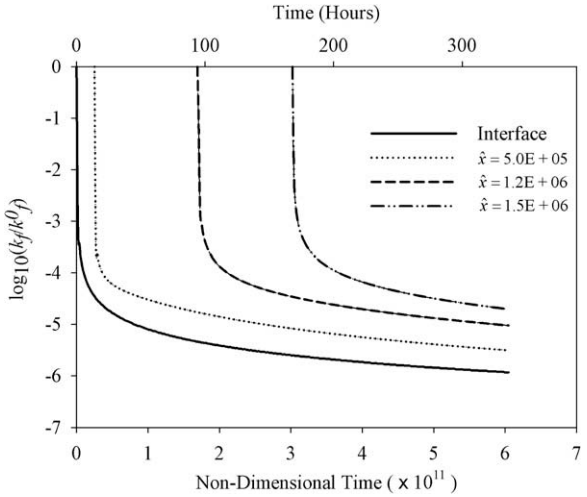

Fig. 4. Oxidation reaction rate constant (normalized) versus time at d within the scale layer.

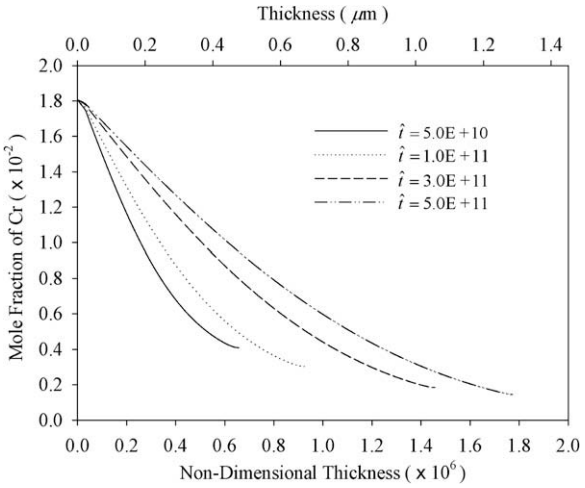

Fig. 5. Distribution of Cr ion across the scale thickness at different time.

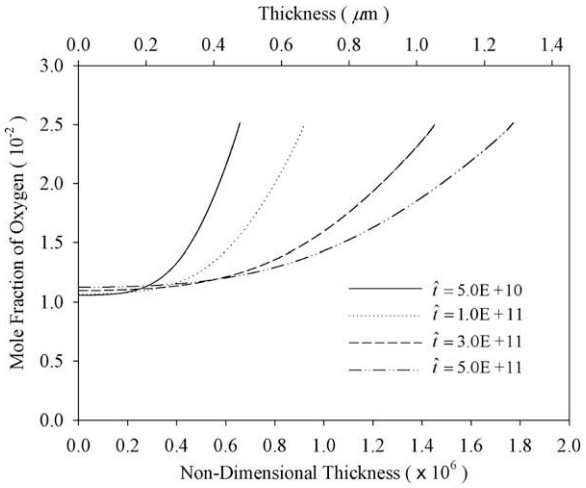

Fig. 6. Distribution of O ion across the scale thickness at different times.

rate starts at a higher value, decreases very quickly to almost zero. This is consistent with the stress distribution shown in Fig. 3a and b, i.e., compressive stress in the oxide grows rapidly to prohibit further internal oxidation. Consequently, new oxide grows primarily on the air–scale interface, which is consistent with experimental observations (Brylewski et al., 2001) that Cr ion diffusion is predominant in the oxide layer for Cr–Fe alloys. In fact, if new oxide is formed primarily on air–scale interface, there must be strong upward diffusion of Cr ions. This can also be seen from the Cr ion distribution across the scale thickness as shown in Fig. 5. Because of the prescribed constant supply of Cr atoms at the metal substrate, the concentration of Cr ion in the scale layer near the scale–metal interface is the highest and remains constant, $c_{Cr} \approx 0.018$. Cr ion concentration is the lowest near the air–scale interface, and continuously decreases with time.

On the other hand, the oxygen ion concentration is the lowest ($c_O \approx 0.012$) at the scale–metal interface, and remain almost constant for about 1/3 of the scale thickness, as shown in Fig. 6a. It then increases quickly towards the air–scale interface and reaches the prescribed $c_O = 0.025$, a value dictated by the prescribed oxygen partial pressure $P_{O_2} = 0.3$ and (36).

To further understand the oxidation kinetics, upward motion velocity of the oxide lattice $\hat{u}_3(\hat{x}_3, \hat{t})$ is plotted in Fig. 7 across the scale-layer thickness at different times. It is seen that after about 100 h, the oxide lattice over much of the scale-layer no longer move upward anymore. In other words, convective motion of the lattice due to internal oxidation is significant only very near the air–scale interface. This also implies that internal oxidation eventually becomes insignificant over long time oxidation, and the growth of new oxide is primarily at the air–scale interface. The oxidation is thus controlled primarily by the upward diffusion of Cr ions across the scale-layer, and the kinetics becomes parabolic. This is further verified by plotting the parabolic rate constant $k_p = \hat{h}^2/\hat{t}$, see Fig. 8. It is

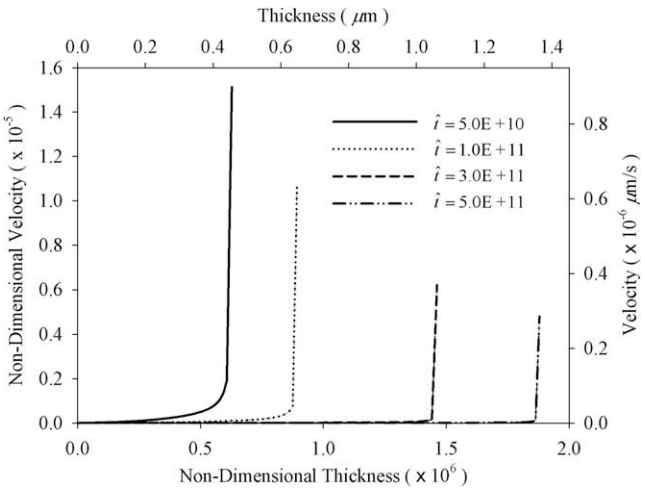

Fig. 7. Distribution of oxide velocity across the scale thickness at different times.

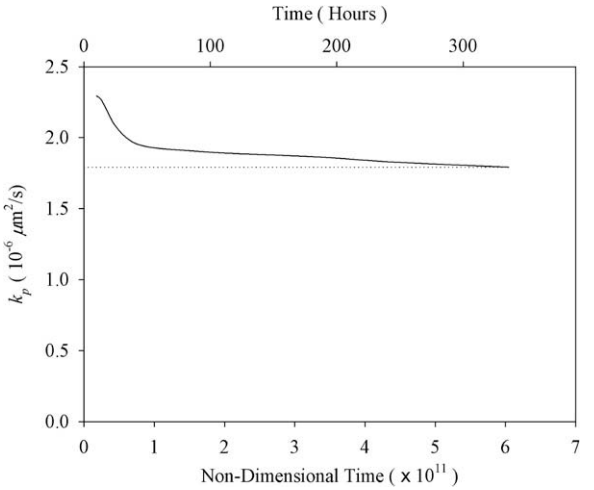

Fig. 8. The evolution of k_p over time.

seen that the kinetics is not parabolic in the early stage of oxidation.

7. Summary remarks

In this paper, a continuum thermodynamic model is developed to account for stress–diffusion interaction in the oxidation of Cr–Fe alloys. In comparison with other existing models, the present approach is formulated in the Eulerian framework. One of the advantages of the Eulerian formulation is to allow the oxide lattice to "flow" upward, avoiding the complexity of computing the velocities of metal–scale and scale–air interfaces and greatly simplifying the equations and the numerical solution. Another important advance is the use of a fully coupled theory (Swaminathan et al., 2007) between chemical reaction and mechanical stress, namely not only oxidation induces stress, but in return stress also affects the rate of oxidation. In this fully coupled theory, not only the hydrostatic stress, but also the deviatoric stress needs to be considered. The model provides detailed distribution of stresses in the scale layer, as well as concentration distributions of all diffusing species in the system. The model results provide clear insight of oxidation mechanisms and how the stress affects the diffusion and oxidation process. It is found that the distribution of stress and the concentration of diffusible species can be scaled by the oxidation reaction rate constant. This means that, with proper scaling, the numerical results in the dimensionless form can be used for any value of the reaction rate. Finally, it should be point out that, although it is developed based on a Cr–Fe alloy, the present model can be easily extended to many different types of binary alloys.

Acknowledgements

The work was supported in part by the National Science Foundation (CMMI 0726286). Initial financial support by Pacific Northwest National Lab and discussions with Drs. M. Khaleel and X. Sun are also acknowledged.

References

Atkinson, A., 1985. Transport processes during the growth of oxide films at elevated temperature. Reviews of Modern Physics 57, 437–470.
Brylewski, T., Nanko, M., Maruyama, T., Przybylski, K., 2001. Application of Fe–16Cr ferritic alloy to interconnector for a solid oxide fuel cell. Solid State Ionics 143, 131–150.
Cabrera, N., Mott, N.F., 1948. Theory of the oxidation of metals. Reports on Progress in Physics 12, 163–184.
Clarke, D.R., 2003. The lateral growth strain accompanying the formation of a thermally grown oxide. Acta Materialia 51, 1393–1407.
Dechamps, M., Barbier, F., 1991. Science of Ceramic Interfaces. Elsevier, Holland.
Garcia, E.A., Kovacs, J., 1994. Diffusion model for the oxidation of zirconium at 573 and 623 K. Journal of Nuclear Materials 210, 78–83.
Hammer, J.E., 2002. The Oxidation of Materials for Interconnects in Solid Oxide Fuel Cells. University of Pittsburgh, Pittsburgh.
Horiguchi, K., Shindo, Y., 2003. Experimental and theoretical results for bending of a soft ferromagnetic plate in a transverse magnetic field. Acta Mechanica 162, 185–194.
Hoshino, K., Peterson, N.L., 1985. Cation self-diffusion and impurity diffusion in Fe_2 O_3^+. Journal of Physics and Chemistry of Solids 46, 1247–1254.
Hultquist, G., Seo, M., Sato, N., 1986. Selective oxidation of Fecr alloys in the 295–450 K temperature-range. Oxidation of Metals 25, 363–372.
Huntz, A.M., 1988. Scale growth and stress development, London, UK, pp. 1079–1088.
Huntz, A.M., 1995. Stresses in NiO, Cr_2O_3 and Al_2O_3 oxide scales. Materials Science & Engineering A: Structural Materials: Properties, Microstructure and Processing A201, 211–228.
Kofstad, P., 1989. Fundamental Aspects of Corrosion by Hot Gases. Les Embiez, France. pp. 25–29.
Krishnamurthy, R., Srolovitz, D.J., 2003. Stress distributions in growing oxide films. Acta Materialia 51, 2171–2190.
Krishnamurthy, R., Srolovitz, D.J., 2004. Stress distributions in growing polycrystalline oxide films. Acta Materialia 52, 3761–3780.
Kurokawa, H., Kawamura, K., Maruyama, T., 2004. Oxidation behavior of Fe–16Cr alloy interconnect for SOFC under hydrogen potential gradient. Solid State Ionics 168, 13–21.
Levich, V., 1962. Physicochemical Hydrodynamics. Prentice-Hall, Englewood Cliffs, N.J.
Limarga, A.M., Wilkinson, D.S., Weatherly, G.C., 2004. Modeling of oxidation-induced growth stresses. Scripta Materialia 50, 1475–1479.
Lobnig, R.E., Schmidt, H.P., Hennesen, K., Grabke, H.J., 1992. Diffusion of cations in chromia layers grown on iron-base alloys. Oxidation of Metals 37, 81–93.
Noden, J.D., Knights, C.J., Thomas, M.W., 1968. Growth of austenitic stainless steels oxidised in carbon and oxygen bearing gases. British Corrosion Journal 3, 47–55.
Pieraggi, B., Rapp, R.A., 1988. Stress generation and vacancy annihilation during scale growth limited by cation-vacancy diffusion. Acta Metallurgica 36, 1281–1289.
Rhines, F.N., Wolf, J.S., 1970. Role of oxide microstructure and growth stresses in the high-temperature scaling of nickel. 1, 1701–1710.
Seo, M., Hultquist, G., Baba, F., Sato, N., 1986. Selective oxidation of Fe–30Cr at low-temperatures – 743–823-K. Oxidation of Metals 25, 164–174.
Stringer, J., 1970. Stress generation and relief in growing oxide films. Corrosion Science 10, 513–543.
Swaminathan, N., Qu, J., 2009. Evaluation of thermomechanical properties of non-stoichiometric gadolinium doped ceria using atomistic simulations. Modelling and Simulation in Materials Science and Engineering 17.
Swaminathan, N., Qu, J., Sun, Y., 2007. An electrochemomechanical theory of defects in ionic solids. I. Theory. Philosophical Magazine 87, 1705–1721.
Tsai, S.C., Huntz, A.M., Dolin, C., 1996. Growth mechanism of Cr_2O_3 scales: oxygen and chromium diffusion, oxidation kinetics and effect of yttrium. Materials Science & Engineering A: Structural Materials: Properties, Microstructure and Processing A212, 6–13.
Wood, G.C., Hodgkies, T., Whittle, D.P., 1966. A comparison of scaling behaviour of pure iron–chromium and nickel–chromium alloys in oxygen. Corrosion Science 6, 129.
Yoshimura, K., Shindo, Y., Horiguchi, K., Narita, F., 2004. Theoretical and experimental determination of magnetic stress intensity factors of a crack in a double cantilever beam specimen. Fatigue and Fracture of Engineering Materials and Structures 27, 213–218.